CHAPTER 4

EXPLORING PHOTOBIOLOGY AND BIOSPECTROSCOPY WITH THE SAC-CI (SYMMETRY-ADAPTED CLUSTER-CONFIGURATION INTERACTION) METHOD

JUN-YA HASEGAWA[1] AND HIROSHI NAKATSUJI*[2]

[1] *Department of Synthetic Chemistry and Biological Chemistry, Graduate School of Engineering, Kyoto University, Katsura, Nishikyo-ku, Kyoto 615-8510, Japan*

[2] *Quantum Chemistry Research Institute, Kyodai Katsura Venture Plaza 106, Goryo Oohara 1-36, Nishikyo-ku, Kyoto 615-8245, Japan*

Abstract: Recent SAC-CI applications to photobiology and biospectroscopy were summarized. The SAC-CI method is an accurate electronic-structure theory for the ground, excited, and ionized states of atoms and molecules in various spin multiplicities. The present SAC-CI code is available in Gaussian 03 and is applicable to moderately large systems. The recent topics covered in this review are (i) Circular dichroism (CD) spectrum of a nucleoside, uridine, (ii) photo-cycle of phytochromobilin in phytochrome, (iii) excited states and electron-transfers in bacterial photosynthetic reaction centers, (iv) color-tuning mechanism of retinal proteins, (v) excitation and emission of green fluorescent proteins (GFP), and (vi) emission color-tuning mechanism of firefly luciferin. These successful applications show that the SAC-CI method is a useful and reliable tool for studying molecular photobiology and biospectroscopy

Keywords: SAC-CI, Excited State, Photo-Biology, Biospectroscopy, Circular Dichroism, Phytochrome, Photosynthetic Reaction Center, Electron Transfer, Color-tuning Mechanism, Retinal Protein, Green Fluorescent Protein, Firefly Luciferase

4.1. INTRODUCTION

Light is indispensable for life. Green plants and some bacteria use solar energy for the *energy source* in their photosynthesis [1–3]. Archeal bacteriorhodopsin is a membrane bound protein and works as a light-driven proton pump [4, 5]. Another role of light is *information carrier* that is recognized in vision and photo-sensors.

*Corresponding author, e-mail: h.nakatsuji@qcri.or.jp

M. K. Shukla, J. Leszczynski (eds.), Radiation Induced Molecular Phenomena in Nucleic Acids, 93–124.

Our retina has red, green, and blue cones which include rhodopsins as photo-receptors [6–8]. Phytochromes are photo-sensors of green plants [9]. Biological luminescences from fireflies [10] and some jellyfishes [11] are also beautiful activities of living organism. Recently, fluorescent proteins are routinely applied as molecular markers for gene expression in the field of molecular biology [12].

These photobiological events occur as photochemical reactions in proteins. The key steps of the reactions are electronic excitations, electron transfers, structural relaxations, and emissions of photo-functional pigments involved in proteins. Proteins must therefore play important roles for adjusting not only the ground electronic structure but also the excited electronic structure of the functional pigments. Interactions between the ground and excited pigments and the protein environment would be important for controlling the function. To figure out the mechanism of the photo-functions and further to control them, if possible, it is important to elucidate detailed electronic structures of the pigments in proteins in both ground and excited states.

Quantum chemistry plays vital central roles in clarifying and understanding the mechanisms of these photobiological events. Electronic structures and transitions of active centers in proteins obey the principles of quantum mechanics, and molecular properties dramatically change after the transitions. In addition, photochemical events in excited states are often transient and sometimes difficult to study in experimental approaches. If an accurate and reliable theory exists and can be applied to photobiological subjects, one can obtain not only rational explanations but also predictions on the photo-functions of the active centers and proteins.

Recent advances in theoretical and computational chemistry opened a door for clarifying the electronic origins and mechanisms of the photobiological phenomena. To obtain reliable understanding on these subjects, a choice of reliable and useful electronic-structure methodology is one of the most crucial aspects in performing theoretical studies. The accuracy and reliability of the method are crucial particularly in photobiology and biospectroscopy, because the energy ranges of the phenomena are relatively narrow in biology. Further, without accuracy and reliability, new predictions are absolutely hopeless. In such critical situations, theories with semi-empirical nature and the time-dependent density functional theory (TDDFT) are difficult to apply, since the error bars of these theories are wider than the typical energy width of the biological phenomena.

The symmetry-adapted cluster (SAC) [13, 14]/SAC-configuration interaction (CI) [15–18] methodology was proposed by Nakatsuji in 1978 and developed in his laboratory [19–22] as an accurate electronic-structure theory for ground and excited states of molecules. The method has been applied so far to more than 150 molecules [19–22] and established as a useful method for studying chemistry and physics involving various electronic states. The analytical energy gradient method for the SAC/SAC-CI energy was developed [23–27]. This is an important tool for geometry optimizations and for studying the relaxation processes of molecules in their excited states. The SAC/SAC-CI code was released through Gaussian 03 program [28]. The SAC/SAC-CI code permits one to do perturbation-selection of linked excitation

operators [29], which permits the method to be applicable to very fine spectroscopy of relatively small molecules to photobiology and biospectroscopy of relatively large molecules.

In this review, we provide an overview of our SAC-CI applications to some important photobiological and biospectroscopic subjects. In Section 4.2, the methodological and the computational aspects of the SAC-CI method are briefly explained. Next, we review some recent SAC-CI applications to circular dichroism (CD) spectrum of a nucleoside, uridine (Section 4.3), structural identification of some key isomers in phytochrome (Section 4.4), (iii) excited states and electron transfer in bacterial photosynthetic reaction centers (Section 4.5), (iv) color-tuning mechanism of retinal proteins (Section 4.6), (v) excited states of green fluorescent protein and its mutants (Section 4.7), and (vi) emission color-tuning of firefly luciferase (Section 4.8). Through these successful applications, we show that the SAC-CI method is a useful tool for the studies in photobiology and biospectroscopy.

4.2. SAC-CI THEORY AND THE COMPUTATIONAL PROGRAM: A BRIEF OVERVIEW

In this section, we explain the SAC-CI method and the computational program. For detailed descriptions, we refer to the original papers [13–18] and the earlier review articles [19–22].

The SAC/SAC-CI method is a correlated electronic-structure theory for the ground and excited states in various spin multiplicities. The SAC method belongs to the coupled-cluster theory [30, 31]. In the case of a closed-shell singlet state, the SAC wave function is written as

$$\Psi_g^{SAC} = \exp\left(\hat{S}\right)|\Psi_0\rangle, \tag{4-1}$$

where Ψ_0 is the reference determinant, and $\hat{S}$ is the linear combination of the excitation operators,

$$\hat{S} = \sum_I C_I \hat{S}_I^\dagger. \tag{4-2}$$

The excitation operator $\hat{S}_I$ is symmetry-adapted, which discriminates between the SAC and ordinary CC methods. The C_I is the coefficient of the operator. Applying the variational principle, we obtain the variational SAC equations.

$$\left\langle \Psi_g^{SAC} \right| \hat{H} - E_g \left| \Psi_g^{SAC} \right\rangle = 0 \tag{4-3}$$

$$\left\langle \Psi_g^{SAC} \right| \left(\hat{H} - E_g\right) \hat{S}_I^\dagger \left| \Psi_g^{SAC} \right\rangle = 0 \tag{4-4}$$

These equations are iteratively solved to determine the energy and the coefficients. The SAC wave functions for open-shell systems were also defined and described

elsewhere [13, 32]. Since the correlation energy calculated by the SAC method is size-extensive, the method is applicable to large systems.

The Eq. (4-4) actually indicates the generalized-Brillouin theorem. This theorem implies that a function $\hat{S}_I^\dagger \left|\Psi_g^{SAC}\right\rangle$ is the basis function for describing the excited states. Let us consider an excited function,

$$\Phi_K = \hat{P}\hat{S}_K^\dagger \left|\Psi_g^{SAC}\right\rangle, \tag{4-5}$$

where $\hat{P}$ is the operator which projects out the ground state SAC wave function. Using Eqs. (4-3 and 4-4), it is easily shown that these functions $\{\Phi_K\}$ satisfy orthogonality and Hamiltonian orthogonality to the ground-state SAC wave function.

$$\left\langle \Phi_K \left|\Psi_g^{SAC}\right\rangle = 0, \quad \left\langle \Phi_K \right| \hat{H} \left| \Psi_g^{SAC} \right\rangle = 0 \right. \tag{4-6}$$

Therefore, the excited state wave function can be described by a linear combination of the basis functions,

$$\Psi_e^{SAC-CI} = \sum_K d_K \Phi_K, \tag{4-7}$$

where d_K is the coefficient of the function. This is the SAC-CI wave function [15–17] which satisfies the correct relationship between the ground and excited states,

$$\left\langle \Psi_g^{SAC} \mid \Psi_e^{SAC-CI} \right\rangle = 0 \text{ and } \left\langle \Psi_g^{SAC} \left|\hat{H}\right| . \Psi_e^{SAC-CI} \right\rangle = 0. \tag{4-8}$$

To determine the SAC-CI coefficients $\{d_K\}$, we applied the variational principle and obtained the variational SAC-CI equation.

$$\left\langle \Phi_K \right| \left(\hat{H} - E_e\right) \left|\Psi_e^{SAC-CI}\right\rangle = 0 \tag{4-9}$$

The Eq. (4-9) is an eigen equation and gives multiple excited states by single diagonalization. The different SAC-CI solutions are therefore orthogonal to each other.

$$\left\langle \Psi_f^{SAC-CI} \mid \Psi_e^{SAC-CI} \right\rangle = 0 \text{ and } \left\langle \Psi_f^{SAC-CI} \left|\hat{H}\right| \Psi_e^{SAC-CI} \right\rangle = 0. \tag{4-10}$$

In the SAC-CI equations described above, the symmetries of the excitation operators were implicitly limited to be the same as those in the ground SAC wave function. However, the Eqs. (4-5–4-10) were also valid for the excitation operators having different symmetries.

$$\Phi_K = \hat{P}\hat{R}_K^\dagger \left|\Psi_g^{SAC}\right\rangle \tag{4-11}$$

Now, the $\hat{R}_K^{\dagger}$ operator is not only singlet excitations but also triplet, doublet (ionized and electron-attached), and higher-spin multiplicities. Thus, the SAC-CI method can calculate the ground and excited states in various spin-multiplicities.

These formulations based on the variation principle provided the beautiful equations for the ground and excited states. However, in a practical point of view, it is very difficult to solve the Eqs. (4-3, 4-4, and 4-9), since the exponential expansions reach full-CI limit. We introduced non-variational equations for the SAC method,

$$\left\langle \Psi_0 \left| \hat{H} - E_g \right| \Psi_g^{SAC} \right\rangle = 0 \tag{4-12}$$

$$\left\langle \Psi_0 \left| \hat{S}_I \left(\hat{H} - E_g \right) \right| \Psi_g^{SAC} \right\rangle = 0, \tag{4-13}$$

and for the SAC-CI method,

$$\left\langle \Psi_0 \right| \hat{R}_K \left(\hat{H} - E_e \right) \left| \Psi_e^{SAC-CI} \right\rangle = 0. \tag{4-14}$$

These equations are obtained by projecting the Schrödinger equation onto the space spanned by the linked configurations. Since the solutions of the non-variational equations are close to the full-CI ones [33], the deviation between the variational and non-variational solutions would be small for the molecules in the equilibrium structures. These non-variational equations were used for solving the SAC and SAC-CI wave functions in the actual applications.

There is no restriction in the order of the excitation operators in the SAC and SAC-CI theories. The SAC/SAC-CI solutions become exact, if one includes the excitation operator up to the full-CI limit. This implies that the accuracies of the SAC and SAC-CI solutions can be improved systematically by including the higher-order excitation operators. This is one of the great advantages of the SAC/SAC-CI method over DFT. For the practical calculations, there are two standards with respect to the excitation operators in the SAC-CI wave function. For calculating one-electron excitation, ionization, and electron-attachment processes, it is sufficient to include singles and doubles linked excitation operators in the SAC-CI wave functions (SAC-CI SD-*R* method) [19–22]. For describing many-electron processes like shake-up ionizations, we must include higher-order excitation operators in the SAC-CI linked operators, which is the general-*R* method [18]. This approach has been successfully applied to the valence ionization spectra with satellites, molecular structure of multi-electron processes, and the excited states of open-shell systems [21].

The computational code for the SAC and SAC-CI methods was completed in 1978 [16, 17] and published in 1985 (SAC85) [34]. In 2003, the SAC-CI code was incorporated into the Gaussian03 program package [28]. Figure 4-1 overviews the available functions of the SAC-CI program in Gaussian03. Using this code, we can calculate the electronic structures and energy gradients of any ground and excited states from singlet to septet spin multiplicities in both SAC-CI SD-*R* and general-*R* accuracies. To study molecular structures, chemical reactions, and dynamics

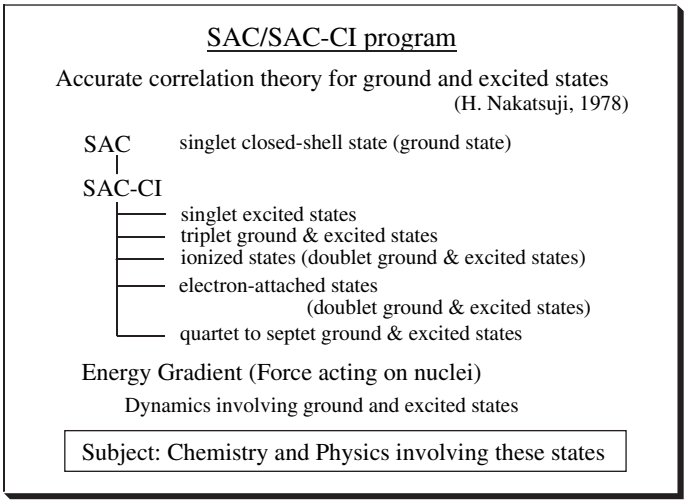

Figure 4-1. Current SAC-CI program system released in Gaussian 03

involving the excited states, we implemented SAC-CI energy gradient (force acting on nuclei) for any of these electronic states [23–27].

In order to calculate larger systems of our research interest, the SAC-CI program adopted a perturbation-selection method [29]. By evaluating the perturbation energy at the second-order level, important double-excitation operators are selected for the SAC and SAC-CI wave functions. This method reduces the number of doubles without losing much accuracy. Owing to these advantages, the SAC-CI method has been successfully applied to the biological systems. In the Gaussian03 program [28], we prepared three levels of energy thresholds: LevelOne, LevelTwo, and LevelThree. LevelThree (default) uses (1×10^{-6} au, 1×10^{-7} au) for (ground, excited) states. LevelTwo and LevelOne are defined as (5×10^{-6} au, 5×10^{-7} au) and (1×10^{-5} au, 1×10^{-6} au), respectively. The LevelThree calculation is the most accurate of the three and is used as the default condition. Calculations with the lower levels are more approximate but computationally easier to apply the SAC-CI method to larger systems. We generally observed that the relative energies among the excited states were rather insensitive among these three threshold sets.

We introduced a new algorithm and succeeded in reducing the computation time for the perturbation selection [35]. In Table 4-1, we show the timing data. The new algorithm was compared with the previous one adopted in the Gaussian 03 rev. C02. The system is a chromophore of Cyan Fluorescent Protein (CFP), $C_{15}H_{15}N_3O_2$(C_1-symmetry). A DZP basis sets [36] was used, and total 290 active orbitals (51 occupied and 239 unoccupied orbitals) were correlated in the SAC/SAC-CI calculation. The number of the reference states was 8 in the selection. The comparison shows that the CPU time was remarkably reduced for singlet and triplet excited states. The present selection algorithm was released in the Gaussian03 rev. D01.

Table 4-1. CPU time for the perturbation selection. Cyan Fluorescent Protein, $C_{15}H_{15}N_3O_2$ (C_1-symmetry), with DZP level basis sets. The 1s core and corresponding virtual orbitals were frozen. Total number of active space is 290 (51 occ. & 239 unocc.)

	CPU time (with HP DS25)	
	Integral sorting	Selection
Singlet ground states		
Previous	none	3m 25s
Present	1m 30s	48s
Singlet excited states		
Previous	none	1h 53m 10s
Present	1m 38s	6m 7s
Triplet states		
Previous	none	6h 47m 53s
Present	1m 37s	11m 48s

4.3. NUCLEOSIDE: CIRCULAR-DICHROISM SPECTRUM OF URIDINE

Photochemical properties of nucleic acids, DNA and RNA, are of great interest not only in biology [3, 37–39] but also in material science [40]. There are many experimental and theoretical studies on the excited states of nucleic acids (for review, see refs. [38, 39]). Since nucleosides and nucleotides are chiral molecules, Circular-Dichroism (CD) spectroscopy is a useful tool to identify the excited states having very small intensity in the ordinary absorption spectrum. CD spectra of DNA are also used for identifying the helical structures [41]. The CD signal is, however, composed of both positive and negative peaks. Without accurate theoretical calculations, it is often difficult to assign the spectrum. As shown in Figure 4-2(a), the experimental absorption spectrum of uridine shows two peaks at 260 (4.77 eV) and 205 nm (6.05 eV) [42]. The experimental CD spectrum has four peaks at 267 nm (peak I, 4.64 eV), 240 nm (peak II, 5.17 eV), 210 nm (peak III, 5.90 eV), and 190 nm (peak IV, 6.53 eV) [42] as shown in Figure 4-2(b). Compared to the absorption spectrum, the peak positions observed in the CD spectrum shift by 0.13∼0.15 eV. Moreover, the CD spectrum in $\lambda_{max} > 240$ nm range is so different from the absorption spectrum.

SAC-CI method was applied to calculate the electronic CD spectrum of uridine [43]. Based on theoretical CD and absorption spectra, observed peaks in the experimental spectra were assigned. The rotational strength (R) in the length form [44] was calculated as imaginary part of the inner product of the electric transition dipole moment (ETDM) and magnetic transition dipole moment (MTDM).

$$R_{ab} = \mathrm{Im}\left[\langle \Psi_a | \hat{\mu} | \Psi_b \rangle \langle \Psi_b | \hat{m} | \Psi_a \rangle\right] \tag{4-15}$$

The ETDM and MTDM were calculated using the SAC and SAC-CI wave functions. $\hat{\mu}$ and $\hat{m}$ are electric and magnetic dipole moment operators, respectively.

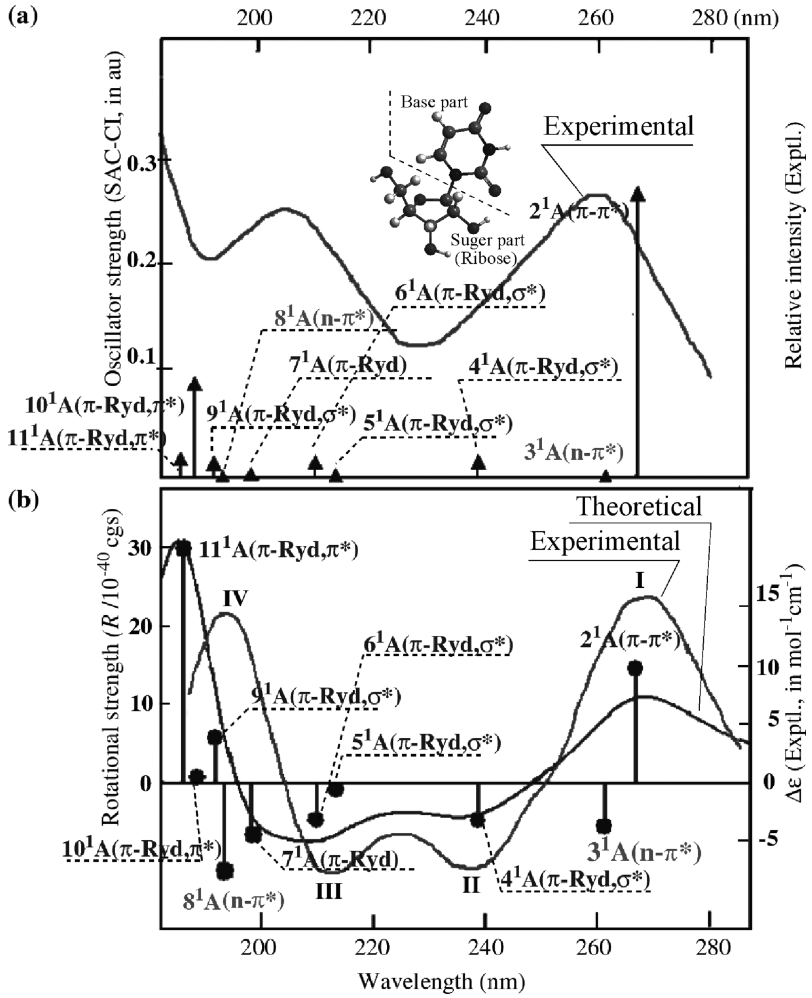

Figure 4-2. (a) Absorption and (b) CD spectra of uridine. In the theoretical CD spectrum, the calculated rotational strengths (*solid vertical lines*) were convoluted with the Gaussian envelopes

Since the rotational strength includes the MTDM, the CD spectrum can detect excited states having little oscillator strength in the absorption spectrum. For computational model, the OH and hydroxymethyl groups in the sugar ring are substituted by the H atoms. Geometry was optimized at DFT(B3LYP [45, 46])/6-31G* [47, 48] level. For calculating the excited states and CD spectrum, the basis functions employed were TZ [49] with double polarization functions [50] plus double Rydberg functions [36] for every C, N and O atoms in the base part. The DZ [36, 51] sets were used for the other atoms. In addition, double Rydberg d-functions [36] were placed on the center of the base ring. In the SAC-CI calculation, 1*s* orbitals of the

C, O and N atoms were treated as the frozen orbitals. Perturbation selection [29] was carried out at the "LevelTwo" level of thresholds.

In Figure 4-2, the SAC-CI theoretical spectra are compared with the experimental ones. Excitation energy, second moment, oscillator strength, and rotational strength are summarized in Table 4-2. The intense peak at 260 nm (4.77 eV) in the absorption spectrum was assigned to the 2^1A state (valence $\pi-\pi^*$ excitation). The 3^1A state ($n-\pi^*$ excitation) was located at 4.74 eV. The CD rotational strengths of these states were opposite each other. Although the oscillator strength of the 3^1A state is very small (0.0001 bohr), the calculated rotational strength (-6.42×10^{-40} cgs) is comparable to that of the 2^1A state (17.00×10^{-40} cgs) in magnitude. Since the signs of the rotational strengths are opposite, the two peaks cancel each other. Consequently, the residual positive contribution from the 2^1A state is observed as the positive peak I in the CD spectrum. This cancellation also shifts the peak I to the lower-energy region in the CD spectrum.

Peak II was assigned to the 4^1A state which has negative rotational strength (-5.42×10^{-40} cgs). The nature is a one-electron excitation from π orbital to mixed σ^* and Rydberg orbitals. The 4^1A state could also be ascribed to the shoulder in the high-energy side of the 260 nm peak (4.77 eV) in the absorption spectrum.

Peak III was assigned to the $5\sim7^1$A states having negative rotational strength. Peak IV in the CD spectrum would be ascribed to the positive rotational strength from 9^1A and 11^1A states. Since the excitation energies of the $8\sim11^1$A states were higher than 6.4 eV, these four states would contribute to the broad absorption in this part of the absorption spectrum.

To understand the origin of the rotational strength, we performed factorization analysis for the rotational strength of $\pi-\pi^*$ (2^1A) and $n-\pi^*$ (3^1A) transitions. The

Table 4-2. Singlet excited states of uridine calculated by the SAC-CI method

State	Nature	SAC-CI				Exptl[a]	
		E_{ex}[b]	Sec.[c]	Osc.[d]	Rot.[e]	E_{ex}(abs)[f]	E_{ex}(CD)[g]
X^1A	Ground State	–	−170	–	–	–	
2^1A	$\pi-\pi^*$	4.64	−171	0.2875	17.00	4.77	4.64(+)
3^1A	n-π^*	4.74	−169	0.0001	−6.42		
4^1A	π−(Ryd,σ^*)	5.19	−228	0.0153	−5.42		5.17(−)
5^1A	π−(Ryd,σ^*)	5.80	−241	0.0008	−1.00		
6^1A	π−(Ryd,σ^*)	5.90	−266	0.0144	−5.46	6.05	5.90(−)
7^1A	π−Ryd	6.24	−282	0.0026	−7.83		
8^1A	n-π^*	6.40	−167	0.0004	−13.12		
9^1A	π−(Ryd,σ^*)	6.45	−276	0.0132	6.84		
10^1A	π−(Ryd,π^*)	6.57	−240	0.0944	0.75	>6.5	6.53(+)
11^1A	π−(Ryd,π^*)	6.66	−261	0.0182	34.57		

[a] Reference [42]; [b] Excitation energy in eV; [c] Electronic second moment in bohr^2; [d] Oscillator strength in bohr; [e] Rotational strength in 10^{-40} cgs unit; [f] Peak maximum in the absorption spectrum [42]; [g] Peak maximum in the CD spectrum [42]. Sign in the parenthesis denotes the sign of the rotational strength.

rotational strength can also be expressed by using the angle θ between ETDM and MTDM.

$$R_{ab} = \mathrm{Im}\left[\left|\vec{\mu}_{ab}\right|\left|\vec{m}_{ab}\right|\cos\theta\right] \tag{4-16}$$

This analysis classifies the origin of the rotational strength in terms of the magnitudes of the two transition moments and their angle. The latter determines the selection rule of the optical activity. In the case of the $\pi-\pi^*$ transition (2^1A state) of uridine, the angle between $\vec{\mu}$ and $\vec{m}$ is almost orthogonal (89.07°). Although the cosine part is very small, both ETDM and MTDM contribute to the rotational strength. On the other hand, both ETDM and MTDM are small in the $n-\pi^*$ transition (3^1A state). However, the angle θ (127.08°) significantly deviates from 90°, which is large enough to be observed in the CD spectrum. The reason of the deviation is in the character of the *n*-orbital. Although the π and π^* orbitals of uridine are localized in the uracil moiety, the *n*-orbital has certain amount of amplitude in the sugar part of uridine. The rotational strength of the $\pi-\pi^*$ transition originates from the magnitude of the transition dipole moments, and that of the $n-\pi^*$ transitions from the symmetry-lowering.

4.4. ON THE PHOTO-CYCLE OF PHYTOCHROME: STRUCTURE OF P_f AND P_{fr} FORMS OF PHYTOCHROMOBILIN (PΦB)

A biliprotein Phytochrome is one of the most important photoreceptors in green plants [9] and controls the photo-morphogenic processes. Phytochrome exists in one of two photo-interconvertible forms: physiologically inactive P_r and active P_{fr} forms which absorb light in the red ($\lambda_{max} = 668$ nm, 1.86 eV) and in the far-red ($\lambda_{max} = 730$ nm, 1.70 eV) regions, respectively [52]. The absorption of light initiates the photoisomerization of phytochromobilin (PΦB, Figure 4-3) included in phytochrome. Several transient intermediates between the P_r and P_{fr} forms were also detected and monitored by UV/vis spectroscopy [53]. Resonance Raman spectroscopy [54–59] was used for studying the structure of PΦB. Kneip et al. proposed that PΦB in the P_r form is in ZZZasa (C_5-Z, C_{10}-Z, C_{15}-Z, C_5-anti, C_{10}-syn, C_{15}-anti) structure [59], while Andel III et al. reported that the P_r and P_{fr} forms are ZEZaas and ZEEaaa isomers, respectively [56]. However, the crystal structure of the phytochrome has not yet been obtained.

In such a situation, reliable theoretical studies on the absorption spectra would provide useful information on the relationship between the structure and the absorption spectrum. As shown in Figure 4-3, three models, A1, A2, and B, were examined for the photo-isomerization. The Models A1 and A2 were based on the Resonance Raman study by Kneip et al [59]. For Model A2, we also referred to a study by Lippitsch et al. [60] in which a rotation around a single bond (C_{14}–C_{15}) was also suggested (Hula Twist). Model B was based on the Resonance Raman study by Andel III and co-workers [56].

In the computational model, substituents that do not conjugate with the π-orbitals were replaced by the hydrogen atoms. We included a propanoic acid that mimics

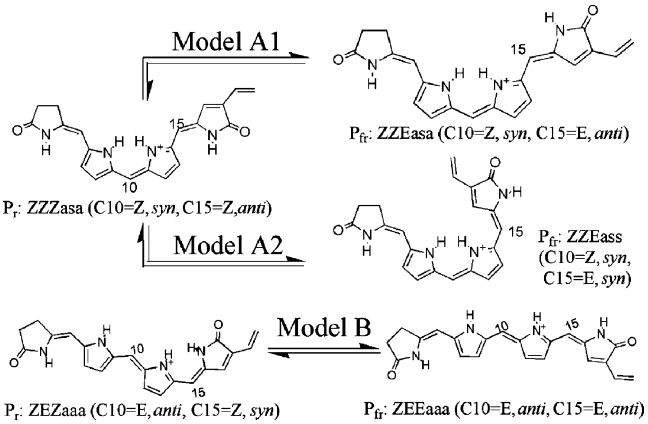

Figure 4-3. Possible mechanisms for the photo-isomerization of phytochromobilin

an acidic residue. We also evaluated protonation states of the N atom in the ring C at DFT [61] (B3LYP [45])/6-31+G(d) level. In Models A1 and A2, the protonated forms (PΦB-H)$^+$-(Asp)$^-$ were more stable than the neutral forms (PΦB)-(Asp-H) by 4.5 and 5.4 kcal/mol, respectively. These results agreed with the experimental findings [55, 56, 59]. However in Model B, the neutral forms of ZEZaas and ZEEaaa isomers were slightly more stable than the protonated ones by 0.7 and 3.4 kcal/mol, respectively. Single-point SAC-CI/DZ calculations were performed for these structures. For the negatively charged oxygen atoms in the aspartate, single *p*-type anion functions ($\alpha = 0.059$) [36] were augmented. The frozen-core approximation was introduced for the 1*s* orbitals of C, N, and O atoms and their corresponding virtual orbitals were also treated as the frozen orbitals. The perturbation selection of the excitation operators [29] was carried out with the LevelTwo set.

As shown in Figure 4-4, the SAC-CI results clearly showed that the spectral change of Model A2 was very close to that of the experiment. The amount of the red-shift was calculated to be 0.11 eV, which was very close to the experimental value (0.16 eV). The calculated excitation energies for ZZZasa and ZZEass structures were 1.73 and 1.62 eV, respectively, which were in reasonable agreement with the experiment [52]. The oscillator strengths of the ZZZasa and ZZEass structures were 1.31 and 0.77 au, respectively, and the change in the spectral intensity was also reproduced. On the other hand, the SAC-CI results for Models A1 and B could not explain the experimental spectra. From these results, we concluded that protonated ZZZasa and ZZEass isomers are assigned to the P_r and P_{fr} forms of PΦB, respectively.

The UV/vis spectroscopy [53, 62] and time-resolved Circular Dichroism (TRCD) [63] studies discovered lumi-R and meta-R_a states as the intermediate states between the P_r and P_{fr} forms. The experimental absorption peak maxima of lumi-R (1.80 eV) and meta-R_a (1.87 eV) states are very close to that of P_r form (1.86 eV) [62]. The C_{15}=C_{16} rotation is so far accepted as the primary step of the photo-isomerization

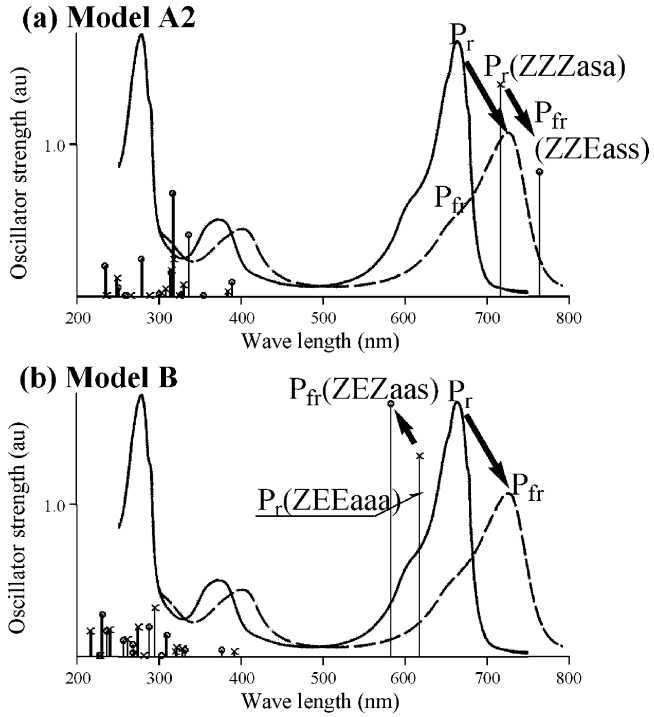

Figure 4-4. (a) SAC-CI spectra for Model A2: ZZZasa (×) and ZZEass (◯) isomers. (b) SAC-CI spectra for Model B: ZEZaas (×) and ZEEaaa (◯) isomers

[64]. Our present result showed that the structure differences between the P_r and P_{fr} forms are both in the C_{15}=C_{16} rotation from Z- to E-conformation and in the C_{14}-C_{15} rotation from anti- to syn-conformation. Therefore, ZZEasa isomer is a possible candidate for the lumi-R or meta-R_a forms. The calculated excitation energy for ZZEasa isomer was 1.71 eV, which was 0.02 eV smaller than that of ZZZasa isomer, P_r form. The result suggested that lumi-R and meta-R_a could have ZZEasa structure as a basic skeleton.

4.5. BACTERIAL PHOTOSYNTHETIC REACTION CENTER: EXCITED STATES AND ELECTRON TRANSFERS

Light-induced transmembrane electron transfer (ET) in the photosynthetic reaction center (PSRC) is a key step of the energy production in the green plants and bacteria [1–3]. The PSRC protein contains seven chromophores: bacteriochlorophyll dimer (Special Pair, **P**), two bacteriochlorophyll monomers ($\mathbf{B_A}$, $\mathbf{B_B}$), two bacteriopheophytin monomers ($\mathbf{H_A}$, $\mathbf{H_B}$), and two quinones ($\mathbf{Q_A}$, $\mathbf{Q_B}$). The chromophore alignment has pseudo-C_2 symmetry as shown in Figure 4-5. The electron transfer in the PSRC is unidirectional and highly efficient [65]. An excited electron at **P** is

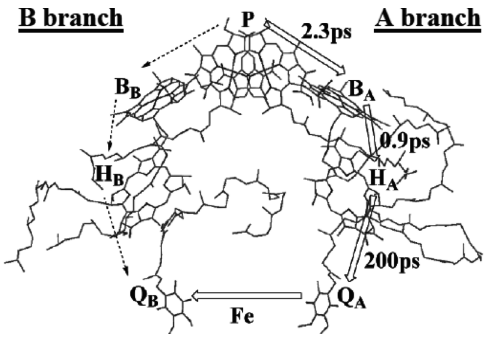

Figure 4-5. Chromophores in the photosynthetic reaction center (PSRC) of *Rb. sphaeroides*

sequentially transferred only along the A-branch in *Rhodobactor (Rb.) sphaeroides* (L-branch in *Rhodopseudomonas (Rps.) viridis*). To investigate the primary photochemical event, the SAC-CI method was applied to the photo-absorption spectrum of the PSRC in *Rps. viridis* [66–68] and *Rb. sphaeroides*[69]. To clarify the unidirectionality of the electron transfer, the SAC-CI wave functions were also used for calculating the electronic factor in the electron-transfer rate constant [66–69]. The initial structure of the PSRC was taken from a X-ray structure (1PRC [70] and 1OGV [71]). The SAC-CI/D95 [36] level calculations was performed for each chromophore. The electrostatic effect from the protein was treated by a point charge model using AMBER force field [72].

The photo-absorption and linear dichroism (LD) spectra of *Rps. viridis* calculated by the SAC-CI method were compared with the experimental data as shown in Figure 4-6. A total of 21 states were calculated in the energy region of 1.3∼2.8 eV. Based on the theoretical spectrum and the other experimental findings, the 14 peaks observed in the experiment were assigned and their characters were clarified. The root mean square (rms) error in the SAC-CI excitation energy was 0.14 eV, indicating that reasonable assignments were obtained [66, 67]. The absorption spectrum of *Rb. sphaeroides* was also assigned with an rms error of 0.11 eV [69]. These assignments provided a starting point for the photochemical studies of the PSRC. The first peak, which is important as the initial state of the ET, is assigned to the first excited state of **P**. The HOMO $\rightarrow$ LUMO excitation is the dominant contributor to the wave function.

Using these SAC-CI wave functions, we calculated the electronic factor $|H_{IF}|^2$ in the ET rate constant.

$$k^{ET} = \frac{2\pi}{\hbar}|H_{IF}|^2\,(FC)\,, \tag{4-17}$$

where FC is Frank-Condon factor which describes the contribution from the nuclear dynamics. The details of the computational procedure are found in the previous paper [68]. The results are summarized in Figure 4-7(a,b). The energy levels of the states were taken from a previous experimental study [73]. In the case of *Rps.*

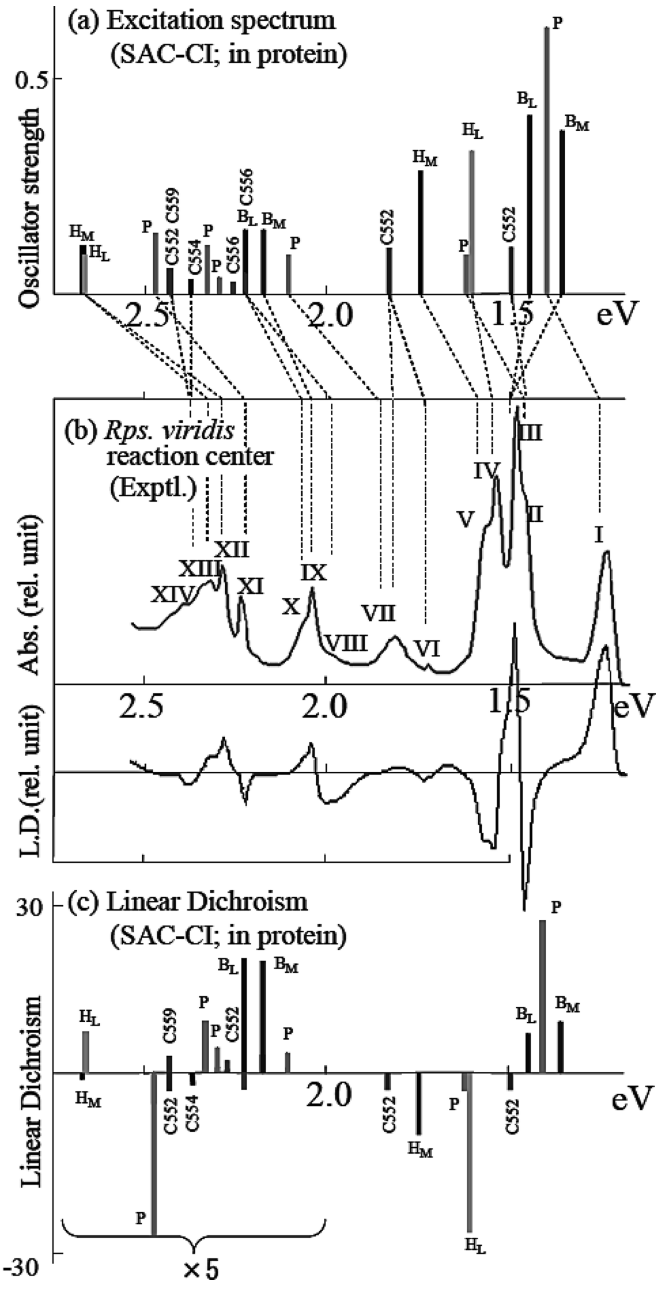

Figure 4-6. Absorption and linear dichroism spectra for the PSRC of *Rps. viridis*. (a) SAC-CI theoretical excitation spectrum [67], (b) Experimental absorption and linear dichroism spectra [146], (c) SAC-CI theoretical linear dichroism spectrum [67]

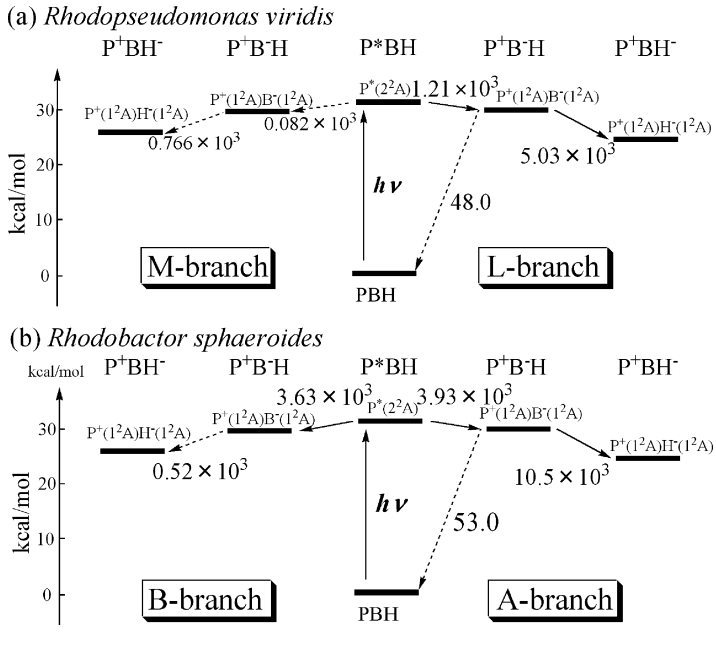

Figure 4-7. Electronic factors in the rate constant calculated for the electron transfers in the bacterial photosynthetic reaction centers of (a) *Rhodopseudomonas viridis*, and (b) *Rhodobactor sphaeroides*

viridis (Figure 4-7(a)), the electronic factor of the ET from **P** to $\mathbf{B_L}$ was 15 times larger than that from **P** to $\mathbf{B_M}$ [66, 68]. We note that $\mathbf{B_L}$, $\mathbf{B_M}$, $\mathbf{H_L}$, and $\mathbf{H_M}$ in *Rps. viridis* are equivalent to $\mathbf{B_A}$, $\mathbf{B_B}$, $\mathbf{H_A}$, and $\mathbf{H_B}$ in *Rb. sphaeroides*, respectively. The ET electronic factor for $\mathbf{B_L} \rightarrow \mathbf{H_L}$ was also larger than that for $\mathbf{B_M} \rightarrow \mathbf{H_M}$ [66, 68]. The unidirectional electron transfer in *Rps. viridis* was explained by the asymmetry in the ET electronic factor. A decomposition analysis revealed that the asymmetric electronic factor has structure-biological origin: the inter-chromophore distance in the L-branch is 0.5 Å shorter than that of the M-branch [66, 68]. In the case of *Rb. sphaeroides*, the calculated electronic factors of the $\mathbf{P} \rightarrow \mathbf{B}$ transfer were very similar between the A- and B-branches as shown in Figure 4-7(b). However, for the ET from **B** to **H**, the electronic factor of the A-branch ET was 20 times larger than that for the B-branch. Therefore, the electronic factor for the $\mathbf{B} \rightarrow \mathbf{H}$ transfer is relevant to the unidirectionality in *Rb. sphaeroides*. We decomposed the electronic factor into the atom-atom contributions. For the ET from $\mathbf{B}_A$ to $\mathbf{H}_A$, the atomic distance of the most contributing pair is 2.95Å, while that of the corresponding pair is 3.96Å in the B-branch. Therefore, the asymmetry in the structure was commonly ascribed to the origin of the unidirectional ET both in *Rps. viridis* and *Rb. sphaeroides*.

We also calculated the electronic factor for the charge recombination $\mathbf{B_A} \rightarrow \mathbf{P}$. As shown in Figure 4-7(a,b). The results were 100 and 200 times smaller than

that of the ET ($\mathbf{B_A} \rightarrow \mathbf{H}$) in *Rps. viridis* and *Rb. sphaeroides*, respectively. This indicated that the electronic factor also controls the efficiency of the ET in the PSRC. It is very interesting to note that the methyl groups play a crucial role in the ET. The decomposition analysis showed that the H atoms of methyl group gives an important contribution [69]. This is due to the hyper-conjugation between the methyl group and the π-system of bacteriochlorophyll skeleton [69]. Such crucial contribution of the hyperconjugation seems to be common to all of the electron transfers in the PSRC, and should be recognized as a general principle.

4.6. RETINAL PROTEINS: COLOR-TUNING MECHANISM

Photo-absorption is the initial event of vision, photo-sensing, and ion-pumps in retinal proteins [4–8, 74, 75]. The absorption maxima are regulated by the protein environment (opsin) and widely spread from 360 to 635 nm [76] to furnish the photo-receptors with the color sensitivity. However, the proteins include a common chromophore, retinal. In order to identify physical mechanism of the color tuning in the retinal proteins, many computational investigations have been performed by using modern quantum-chemistry methodologies [77–87]. Among them, SAC-CI studies gave systematically nice agreement to all of the retinal proteins studied [85–87]. There are important requirements in the computational approach to reproduce the experimental absorption energies. First, to accurately calculate the electronic energy, the electron-correlation should be included appropriately for the ionic $\pi - \pi^*$ excited state of polyene-like molecule [88]. Second, the absorption energy is highly sensitive to the bond-length alternation and the torsional angle of the polyene chain [84, 86]. With Hartree-Fock (HF) optimized geometry, calculated excitation energy significantly overestimates the experimental result [77, 78, 84]. The 2nd order Moller-Plesset (MP2) perturbation theory or B3LYP [45, 46] perform better for the geometry optimization [84, 86]. Third, the interactions between the chromophore and the counter ion must be described properly. Point-charge model lacks the higher-order electronic effects such as electronic polarization, charge-transfer, and exchange interactions [77, 79, 84].

We reported ab initio QM/MM and SAC-CI studies on the color-tuning mechanism of retinal proteins, bacteriorhodopsin (bR) [86], sensoryrhodopsin II (sRII) [86], rhodopsin (Rh) [86], and human blue cone pigment (HB) [87]. The QM(B3LYP/D95(d)) / MM(AMBER99 [89]) geometry optimizations were carried out for the retinal proteins. In Figure 4-8, the structures of the QM segments are illustrated. Active-site (AS) models included counter residues and a water, while retinal (RET) models consisted of only the retinal protonated Schiff-base. The MM segment describes the steric and electrostatic effects of the surrounding environment from the rest of the system by means of the molecular mechanics. With the QM/MM optimized structures, we calculated the absorption energies of the QM segment at the SAC-CI/D95(d) level with the point charges representing the electrostatic field of the surrounding protein.

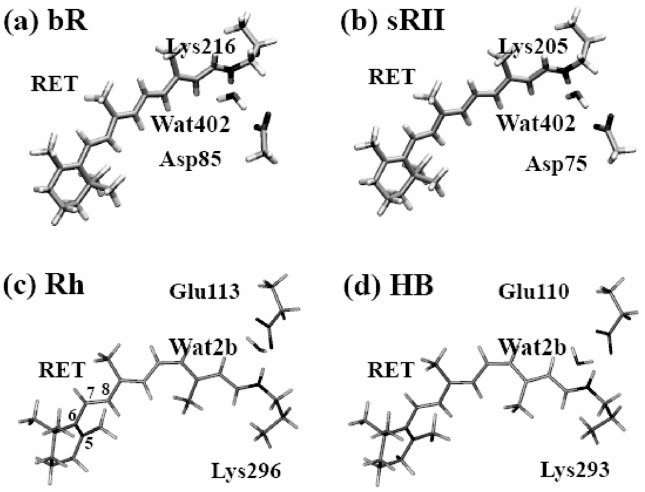

Figure 4-8. QM/MM optimized structures of the active-site of (a) bacteriorhodopsin (bR), (b) sensoryrhodopsin II (sRII), (c) rhodopsin (Rh), and (d) human blue cone pigment (HB). These active-site (AS) models were also used for the QM region in the SAC-CI calculations

In Table 4-3, the SAC-CI results were summarized. The rms deviation between the calculated and experimental absorption energies was 0.09 eV for 6 retinal proteins. TD-B3LYP calculations were also performed with the same geometries. The B3LYP absorption energies for sRII and Rh showed deviations from experiment of 0.15 and 0.07 eV, respectively. However, the deviation in bR was 0.39 eV. TD-DFT results were also qualitatively different from the other methods when the C_6-C_7 bond rotated [84]. Therefore, it would be difficult to use TD-B3LYP method for clarifying the color-tuning mechanism among various retinal proteins.

Mechanism of color-tuning was compared among bR, sRII, and Rh [86]. Absorption energies of both sRII and Rh are 2.49 eV, which is 0.31 eV larger than that of bR. The origin of the spectral blue shifts was decomposed into three contributions. The first one was the structural distortion of the chromophore due to the protein confinement (Structural effect). The second one was the electrostatic (ES) interaction between the chromophore and the surrounding proteins (ES effect). The last one was the quantum effect of the counter-ion and a water molecule in the vicinity of the retinal protonated Schiff base (PSB) (Counter-ion quantum effect). These contributions were deduced from the absorption energies listed in Table 4-3. The structural effect was evaluated as the difference of the absorption energies of the "bare" chromophores.

$$\Delta E^{Struct} = E_{ex}^{RET,bare}(A) - E_{ex}^{RET,bare}(B), \tag{4-18}$$

Table 4-3. The first excited states of rhodopsin (Rh), bacteriorhodopsin (bR), sensoryrhodopsin II (sRII), and human blue cone pigment (HB) calculated by the SAC-CI and other methods

Protein	QM region	Environment	SAC-CI	Exptl.	MRPT2	SORCI	TD-B3LYP
			E_{ex} (eV)	(eV)	E_{ex} (eV)	E_{ex} (eV)	E_{ex} (eV)
bR/WT[f]	AS	in opsin	2.23	2.18[j]	–	–	2.57
	RET		1.88		2.75[d]	2.34[e]	2.49
	RET	bare	1.30	–	2.05[d]	1.86[e]	2.31
bR/R82A[g]	AS	in opsin	2.34	2.23[k]	–	–	–
sRII/WT[f]	AS	in opsin	2.53	2.49[l]	–	–	2.68
	RET		2.17		–	–	2.58
	RET	bare	1.31	–	–	–	2.30
sRII/R72A[h]	AS	in opsin	2.58	2.48[m]	–	–	–
Rh/WT[f]	AS	in opsin	2.45	2.49[i]	2.86[a]	–	2.52
	RET		2.06		2.78[b], 2.59[c]	–	2.44
	RET	bare	1.36	–	2.72[b], 2.72[c]	–	2.53
HB/WT[f]	AS	in opsin	2.85	2.99			
	RET		2.50				
	RET	bare	1.40	–			

[a] CASPT2 result described in ref. [139], [b] CASPT2 result described in ref. [81], [c] CASPT2 result described in ref. [140], [d] MRMP result described in ref. [77], [e] SORCI result described in ref. [84], [f] Shows "Wild Type", [g] Shows "R82A" mutant, [h] Shows "R72A" mutant, [i] Ref. [74, 75, 141], [j] Ref. [142], [k] Ref. [143], [l]Ref. [144], [m] Ref. [145].

where A and B denote the retinal proteins. The ES effect was the difference of the spectral shift due to the electrostatic environment modeled by the point charges.

$$\Delta E^{ES} = \left(E_{ex}^{RET,in\ opsin}(A) - E_{ex}^{RET,bare}(A)\right) - \left(E_{ex}^{RET,in\ opsin}(B) - E_{ex}^{RET,bare}(B)\right) \tag{4-19}$$

The counter-ion quantum effect is the difference of the spectral shift between the AS and RET systems.

$$\Delta E^{Quantum} = \left(E_{ex}^{AS,in\ opsin}(A) - E_{ex}^{RET,in\ opsin}(A)\right) - \left(E_{ex}^{AS,in\ opsin}(B) - E_{ex}^{RET,in\ opsin}(B)\right) \tag{4-20}$$

The dominant contribution in both Rh and sRII turned out to be the ES effect. The amount of the shift in sRII (0.28 eV) is by 0.16 eV larger than that in Rh (0.12 eV). This difference arises from the character of the excited state and the ES potential along the retinal skeleton. The first excited state is characterized as an intramolecular charge-transfer (CT) state. As shown in Figure 4-9(a,b), the HOMO and LUMO are located in the left- and right-halves of the chromophore, respectively. On the other hand, due to the counter ion, the ES potential decreases around the PSB part (Figure 4-9(c)). Therefore, the protein ES effect increases the

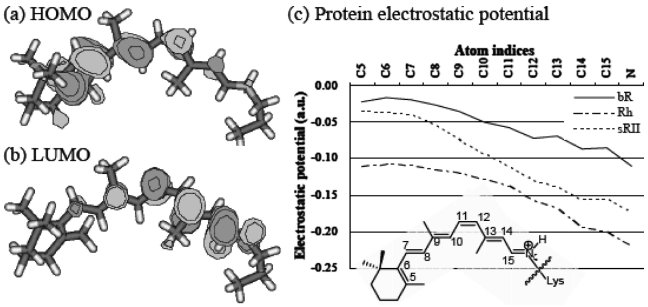

Figure 4-9. (a) HOMO and LUMO distributions of rhodopsin (Rh), (b) Protein-electrostatic potential at atoms in the retinal skeleton in atomic unit

CT excitation energy. The amount of the blue-shift was qualitatively explained by the change in ES potential along the skeleton. This is a general feature seen in the retinal protein including PSB.

The structural distortion effect in Rh (0.06 eV) was larger than that in sRII (0.00 eV). This difference was mainly attributed to the torsion around the C_6-C_7 bond due to the steric repulsion (Figure 4-8(c)). The blue-shift mechanism of human blue-cone pigment (HB) was compared to rhodopsin (Rh) in the same way [87]. As shown in Table 4-3, the ES interaction (0.40 eV) is the dominant contributor to the blue-shift. In order to analyze the ES interaction in more detail, we decomposed the ES interaction into the contribution into each residue [87]. As in the previous experimental studies [90], we found many residues contributing to the blue-shift [91]. Among them, Ser183 and Tyr265 give leading contributions. Compared to Rh, Ser183 and Tyr265 increase HOMO-LUMO gaps of the chromophore by 0.10 and 0.05 eV, respectively. We investigated the protein environment in the vicinity of the retinal SB region of HB and Rh. The O-H bond orientation of Ser183 in HB (Ser186 in Rh) and Tyr265 in HB (Tyr268 in Rh) were significantly different between the two proteins. This is controlled by the hydrogen-bonding network in HB and Rh. Ser289 in HB acts as proton donor, while hydrophobic Ala292 cannot mediate hydrogen-bonding network. Therefore, Ser289 in HB regulates the hydrogen-bonding patterns around the SB region and indirectly contributes to the spectral blue-shift.

4.7. GREEN FLUORESCENT PROTEIN (GFP) AND MUTANTS: PHOTOABSORPTION AND EMISSION ENERGIES

Green Fluorescent Protein is involved in the jellyfish, *Aequorea Victoria* [11, 92–95] and has very efficient emission property. It is now widely used as an excellent molecular marker in various fields of molecular biology [12, 96]. There are theoretical studies investigating spectroscopy [97–104], potential surface of the excited state [105–107], and protein environmental effect [35, 101, 104, 108–110].

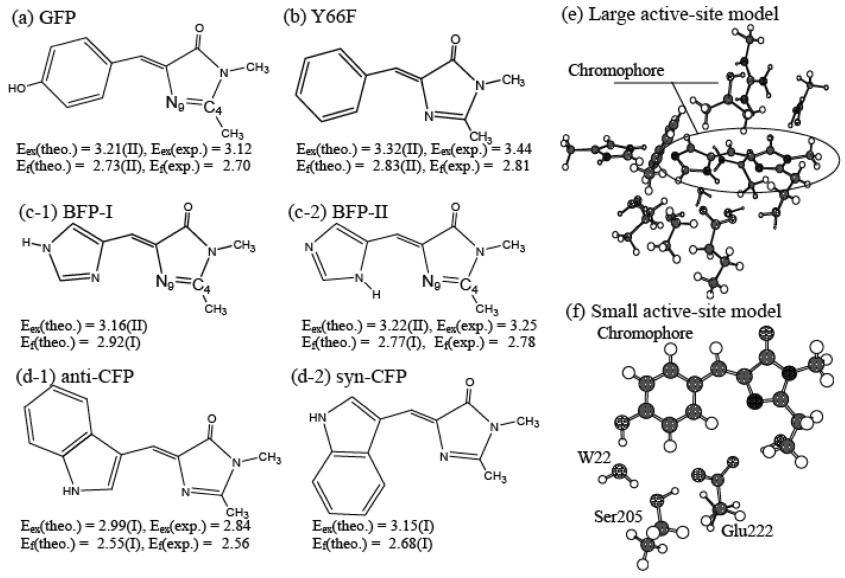

Figure 4-10. Computational models. (a–d) Chromophores of GFP and its mutants. Theoretical and experimental absorption (E_{ex}) and emission energies (E_f) were also indicated. Roman numeral in the parenthesis indicates computational model (see text), (e) Large active site model of BFP for the geometry optimization, (f) Small active site model of GFP for the SAC-CI calculations

We also studied protonation state of GFP chromophore [103] and environmental effect [35].

Several computational models were employed in our study [35]. Model I included a chromophore in gas-phase (Figure 4-10(a–d)). Model II additionally involved a point-charge model for protein electrostatic potential. In Model III, the atoms in the active site (Figure 4-10(f)) were treated by quantum mechanics, and the rest of the protein effect was treated by the point-charge model. The structures used in Models II and III were obtained by using large active-site model (Figure 4-10(e)) at DFT [61](B3LYP [45, 46])/6-31G* [47, 48] and CIS/6-31G* levels for the ground and excited states, respectively.

For the excitation energy of GFP, SAC-CI calculations using Models I, II, and III gave 3.23, 3.21, and 3.27 eV, respectively. These values are reasonably close to the experimental value (3.12 eV [111]). For the fluorescence energy, SAC-CI with Models I and II gave 2.70 and 2.73 eV, respectively. Since the excitation and fluorescence energies obtained by the gas phase model (Model I) and the protein model (Models II and III) were close to each other, the protein environment gives minor contributions to the transition energies. Similar results were obtained for Y66F mutant. We performed a decomposition analysis to clarify the environmental effect [35]. Some neighboring residues, Gln94 and Arg96, decrease the excitation energy [35, 101]. However, the rest of the protein-electrostatic effect increases the excitation energy and diminishes the red-shift effect of Gln94 and Arg96.

Radiating UV (254 nm, 4.9 eV) or visible (390 nm, 3.2 eV) lights induce photochemical conversion of the GFP active site [12, 112, 113]. A charge-transfer (CT) excitation from Glu222 to the GFP chromophore was thought to be a key step in a hypothetical mechanism [113], although there was neither experimental nor theoretical evidences for the CT excitation. We performed SAC-CI calculations for the excited states of GFP active site (GFP-W22-Ser205-Glu222-Ser65, see Figure 4-10(f)) [35]. Such large-scale SAC-CI calculations were performed with an improved code containing a new algorithm for the perturbation selection [35]. Table 4-4 shows singlet and triplet excited states up to 5.5 eV. Since the SAC-CI method can calculate many states distributed in a wide energy region, spectroscopy is one of the best applied fields of the SAC-CI method. The results indicated that a charge-transfer (CT) state is located at 4.19 eV, which could be related to the channel of the photochemistry as indicated in a previous experimental study [113]. On the other hand, there is no CT state below the 2^1A state (3.27 eV). Since GFP has large two-photon absorption cross section [114, 115], the chromophore could be excited to the states around 6.4 eV (3.2 $\times$ 2) by the two-photon processes.

Recent developments realized variety of GFP mutants having different fluorescence colors [12, 96, 116–118]. We studied the excitation and fluorescence energies of Blue Fluorescent Protein (BFP), Cyan Fluorescent Protein (CFP), and Y66F. Protonation state of the chromophore is very important, when the excited-state proton transfer is considered. In the case of BFP, there are two possibilities as indicated in Figure 4-10(c-1 and c-2). Based on the excitation energy, the fluorescence energy, and total energy, we propose that the protonation state of the BFP chromophore is the BFP-II structure. We also calculated the excited state of CFP chromophore in two different conformations as shown in Figure 4-10(d-1 and d-2). The SAC-CI results were close to those of anti-CFP structure. This result agreed with the existing X-ray structure [119].

4.8. RED LIGHT IN CHEMILUMINESCENCE AND YELLOW-GREEN LIGHT IN BIOLUMINESCENCE: EMISSION COLOR-TUNING MECHANISM OF FIREFLY LUCIFERIN

Firefly luminescence is intriguing photobiological phenomenon [10]. The firefly luciferase enzyme (Luc) has also become an important tool for bio-molecular imaging, because of the highly-efficient conversion of chemical energy into light [120]. Therefore, the underlying molecular mechanism of color-tuning must be clarified. In the case of North American firefly (*Photinus Pyralis*), the chromophore, luciferin, is transformed into electronically-excited oxyluciferin ($OxyLH_2$) inside the Luc [121–127], and exhibits the yellow-green emission (556 nm, 2.23 eV). In chemiluminescence (Figure 4-11(b)), keto- and enol-$OxyLH_2$ emit red (620 nm, 1.97 eV) and green (560 nm, 2.20 eV) lights, respectively [125–127]. Because of the similarity, the yellow-green bioluminescence had long been ascribed to the

Table 4-4. Singlet and triplet excited states of the Green Fluorescent Protein active site

State	SAC-CI				Exptl.
	Main configurations (C>0.3)	Character	E_{ex} (eV)[a]	Osc. (au)[b]	E_{ex} (eV)
1^3A	−0.89(103→107)	Cro π → Cro π*	1.77	–	
2^1A	0.90(103→107)	Cro π → Cro π*	3.27	0.56	3.12
2^3A	0.56(101→107)−0.36(103→121)	Cro π → Cro π*	3.71	–	
3^3A	0.79(103→104)	Cro π → Cro Ryd.	3.96	–	
3^1A	−0.90(103→104)	Cro π → Cro Ryd.	3.98	4.0×10^{-3}	
4^3A	0.43(103→104)−0.37(103→105)−0.33(102→107) −0.31(103→110)	Cro π → Cro Ryd.	4.05	–	
5^3A	0.61(99→107)+0.47(98→107)+0.42(97→107)	Cro σ, Glu222→Cro π*	4.09	–	
4^1A	0.84(103→106)−0.38(103→105)	Cro π → Cro Ryd.	4.11	1.7×10^{-3}	
5^1A	−0.61(99→107)−0.47(98→107)−0.42(97→107)	Cro σ, Glu222→Cro π*	4.18	2.7×10^{-2}	
6^3A	0.72(103→106)	Cro π → Cro Ryd.	4.24	–	
6^1A	0.65(103→105)+0.35(103→106)	Cro π → Cro Ryd.	4.34	1.1×10^{-2}	
7^3A	−0.56(103→105)−0.33(101→107)+0.33(102→110)	Cro π → Cro Ryd.	4.47	–	
8^3A	0.60(103→105)+0.36(103→106)	Cro π → Cro Ryd.	4.54	–	
7^1A	0.48(103→105)−0.47(103→110)+0.34(102→107)	Cro π → Cro Ryd.	4.56	1.2×10^{-2}	
8^1A	0.72(101→107)−0.33(103→108)	Cro π → Cro π*	4.85	0.15	
9^1A	−0.75(103→108)−0.31(103→109)	Cro π → Cro Ryd.	4.95	6.8×10^{-3}	
9^3A	0.72(102→107)−0.36(103→110)	Cro π → Cro π*	4.96	–	
10^1A	0.84(103→109)	Cro π → Cro Ryd.	5.17	1.0×10^{-2}	
10^3A	0.66(95→107)	Cro π → Cro π*	5.35	–	
11^1A	0.81(102→106)	Cro π → Cro Ryd.	5.58	8.9×10^{-2}	

[a] Excitation energy in eV unit.
[b] Oscillator strength in atomic unit.

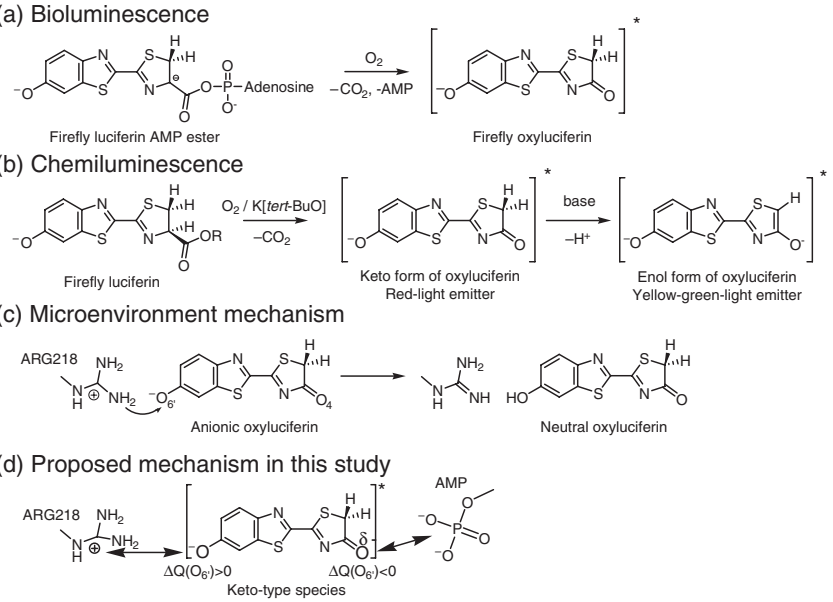

Figure 4-11. Proposed mechanism for (a) bioluminescence and (b) chemiluminescence of the firefly [126]. (c) micro-environment mechanism [136–138, 147], and (d) our mechanism proposed in this study [131]

enol-form of $OxyLH_2$ [125–127]. Recently, Branchini and co-workers found that keto-constrained $OxyLH_2$ shows the yellow-green emission in the Luc [128, 129]. This indicated that the color of the firefly luminescence may be controlled only within the keto-form. We investigated the emission color-tuning mechanism of the firefly luciferin: red light in chemiluminescence and yellow-green light in bioluminescence.

For studying the chemiluminescence in DMSO solution, we examined eight structural isomers and tautomers in different protonation states at SAC-CI /D95(d)//CIS/D95(d) plus PCM(DMSO) [130] level [131]. Counter ion (K^+) included in the experimental solution was explicitly included in the QM calculations. First, we could exclude the neutral forms, keto-s-trans and enol-s-trans, from the candidates for the chemiluminescence emitter, since calculated emission energies were much higher than the observed value [131]. Second, we could also exclude cis isomers, since relative energies were higher than the corresponding trans isomers [131]. Figure 4-12 shows the fluorescence energies of keto-s-trans, enol-s-trans(-1), enol-s-trans(-1)′, and enol-s-trans(-2) forms calculated by the SAC-CI method. Regarding the keto form, the calculated emission energy for keto-s-trans(-1) was 2.10 eV, which agrees reasonably well with the experimental value of 1.97 eV. Thus, keto-s-trans(-1) was confirmed as the red emitter in the chemiluminescence. For the enol form under strongly basic conditions, the calculated

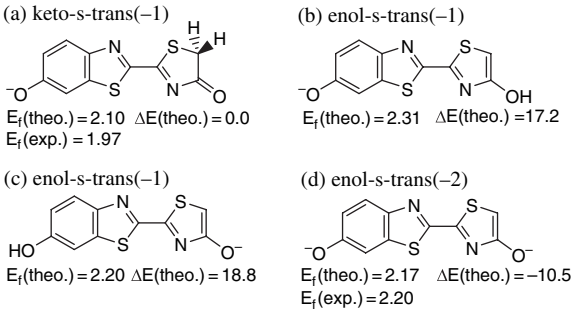

Figure 4-12. Structural of $OxyLH_2$ tautomers in different protonation states. E_f(theo.) and E_f(exp.) denote theoretical and experimental emission energies in eV unit, respectively. ΔE(theo.) denotes relative energy in kcal/mol unit. Keto-s-trans(-1) form was taken as the reference

emission energies of the three candidates, enol-s-trans(-1), enol-s-trans(-1)′, and enol-s-trans(-2), were 2.31, 2.20, and 2.17 eV, respectively [131]. Since all of these values were close to the experimental emission energy of 2.20 eV, we next examined the relative stability of these enol forms in the excited states. The total energy was sum of the energies of potassium-$OxyLH_2$ complex and *tert*-BuO [131]. Since enol-s-trans(-2) was the most stable of the three candidates as shown in Figure 4-12, enol-s-trans(-2) was ascribed to the yellow-green chemiluminescence emitter.

For the bioluminescence, we constructed computational models of $OxyLH_2$–Luc binding complexes using X-ray structure of Luc [132] and a working model proposed by experimental studies [133–135]. These structures were relaxed by performing molecular dynamics, molecular mechanics (MM), and then ab initio CIS (configuration-interaction singles) calculations. In CIS optimization, most of the surrounding residues were treated by quantum mechanics (QM). The 6-31G* [47, 48] sets were used for $OxyLH_2$ and phosphate-group in AMP. The 6-31G sets were used for the others. In the SAC-CI calculations, $OxyLH_2$, the phosphate, Arg218, and His245 were treated by QM. The D95(d) [36] and 6-31G basis sets were used for $OxyLH_2$ and the others, respectively. In both CIS and SAC-CI calculations, electrostatic effect from the other residues was described by the point charges.

In Luc environment, we obtained two representative structures, models A-a and A-b. These two gave the emission energies of 2.33 and 2.08 eV, respectively, as shown in "Calc. III" in Table 4-5. Since these values were close to the experiment (2.23 eV) [128, 129], keto-$OxyLH_2$ in the anionic form (keto-s-trans(-1) in Figure 4-12 (a)) was confirmed to be the yellow-green emitter in Luc environment. The character of the excited state is one-electron transition from HOMO(π) to LUMO(π^*), and these orbitals are clearly localized within $OxyLH_2$.

Next, the possibility of the enol forms was considered. We performed the SAC-CI calculations for enol-s-trans(-1) and enol-s-trans(-2) forms inside Luc. In the

Table 4-5. Emission (fluorescence) energies of $OxyLH_2$ in the keto-s-trans(-1) form in the gas phase and protein environment

Calc.	Environment	QM region	Geom[a]	Emission energy/eV	
				SAC-CI	Exptl.
I		$OxyLH_2$	Gas	1.97	
II	in Gas phase	$OxyLH_2$	A-a	1.73	
			A-b	1.58	
III	in Protein	$OxyLH_2$ + ARG218	A-a	2.33	2.23[b]
		+HIS245 +Phosphate	A-b	2.08	

[a] "Gas" denotes geometry optimized in the gas phase. For structures "A-a" and "A-b", see text; [b] Bioluminescence emission maxima for *Photinus pyralis* wild-type at pH 8.6 [128].

enol-s-trans(-2) structure, the enol group was deprotonated, and the proton was transferred to the phosphate group. The fluorescence energy and energy profile are shown in Figure 4-13(a), together with the optimized structures. The SAC-CI fluorescence energies (data in the parentheses) of keto-s-trans(-1), enol-s-trans(-1), and enol-s-trans(-2) in Luc were 2.33, 2.29, and 2.21 eV, respectively. All of them are close to the experimental value (2.23 eV). However, potential energies of the first excited state of the enol-s-trans(-1) and enol-s-trans(-2) structures are by 19.8 and 34.2 kcal/mol higher than that of the keto-s-trans(-1) structure, respectively. These energy differences are large enough to conclude that the enol transformation is energetically unfavorable in the Luc environment.

Protonation state of the O6′ atom in the benzothiazoryl ring also affects the emission energy [136–138]. We examined another protonation state in which a proton of Arg218 was transferred to $OxyLH_2$ (Figure 4-11(c)). As shown in Figure 4-13(b), the calculated fluorescence energy (3.02 eV) was about 0.8 eV higher than the experimental value. In addition, the total energy evaluated at the CIS/6-31G* level was 20.2 kcal/mol higher than that of the keto-s-trans(-1) system.

We analyzed the origin of the blue-shift by comparing several SAC-CI calculations using different computational models (Table 4-5). The reference gas-phase calculation (Calc. I) gave emission energy of 1.97 eV. In Calc. II, all of the surrounding molecules and the charges were removed from the Calc. III. Difference between Calc. II and Calc. I gives the chromophore structural effect. The fluorescence energies obtained were 1.73 and 1.58 eV for models A-a and A-b, respectively. The structural constraint in the protein environment actually causes red-shifts of 0.24 and 0.39 eV in the fluorescence, respectively. Comparison between Calc. III and Calc. II corresponds to the environmental effect caused by the coulombic interaction between $OxyLH_2$ and the surroundings. This effect leads to a marked blue-shift in fluorescence energy of 0.60 and 0.50 eV in

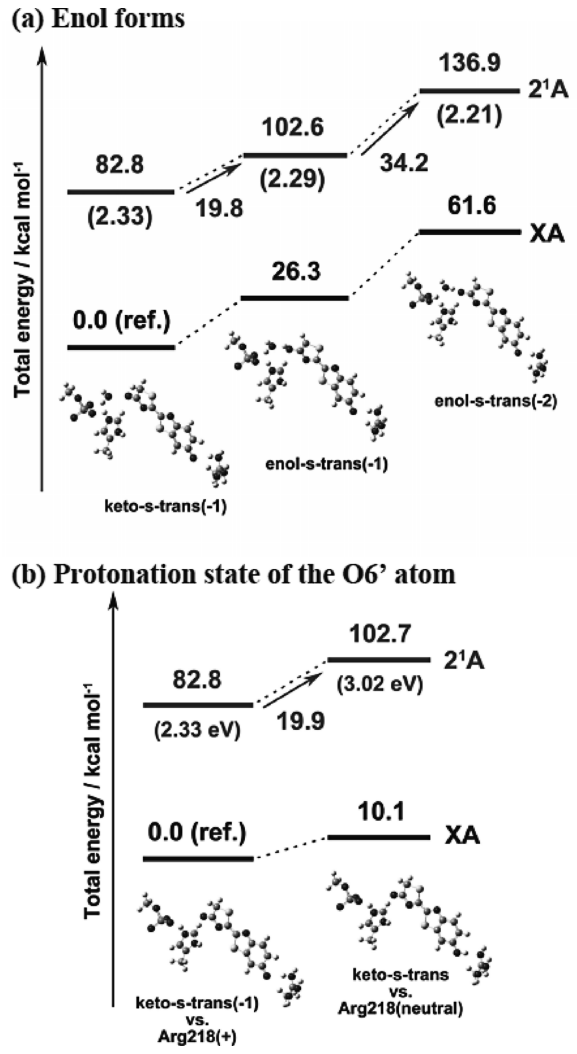

Figure 4-13. (a) Comparison of the potential energy and emission energy (in parenthesis) of the keto and enol forms in the Luc environment, (b) Comparison of the potential energy and emission energy (in parenthesis) of the two protonation states

models A-a and A-b, respectively. A further analysis showed that the blue shift is mainly due to the interactions with Arg218 and phosphate group of AMP. Therefore, we concluded that the emission color of the keto-form remarkably shifts to yellow-green due to the coulombic interaction between $OxyLH_2$ and Luc environment.

4.9. SUMMARY

An overview of the SAC-CI applications to photobiology and biospectroscopy was presented in this account. The most important point in these successful applications would be the accuracy of the SAC-CI theory and computations. A typical example was seen in the retinal proteins. The TD-B3LYP works very nicely for two proteins but gave an error of 0.4 eV in one protein, indicating the method is not systematically applicable to unknown retinal proteins. In Figure 4-14, the SAC-CI results (with DZP basis sets at least) were compared to the experimental data. The molecules included were nucleoside, green fluorescent proteins, retinal protonated Schiff base, and oxyluciferins. The excited states calculated were one-electron $\pi - \pi^*$, n-π^*, $\pi - \sigma^*$ excited states including exciton and intramolecular charge-transfer states. The root mean square (rms) error was 0.09 eV (2.08 kcal/mol) among 26 states. For the chlorophylls in the photosynthetic reaction center and the bilins in phytochrome, the SAC-CI/DZ basis level gave an rms error of 0.13 eV among 26 states. These results indicate the accuracy and reliability

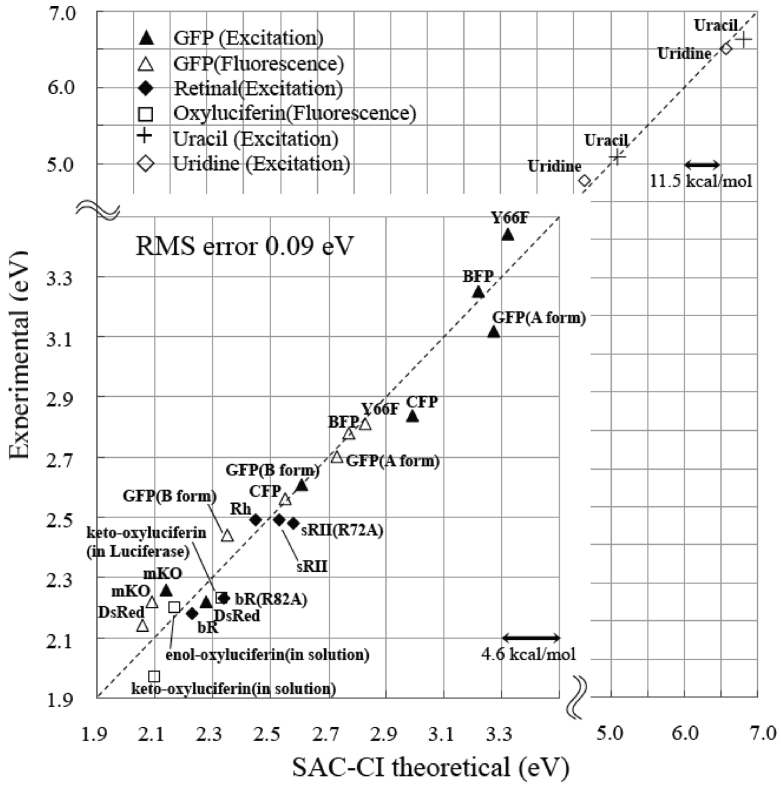

Figure 4-14. Comparison of the SAC-CI and experimental results in some photobiological and biospectroscopic applications

of the excitation/emission energies calculated by the SAC-CI method. For this reason, reliable conclusions could be deduced for spectroscopy, structural identifications, interpretation of the photo-absorption/emission color-tuning mechanisms in photobiology.

ACKNOWLEDGEMENTS

The authors thank Prof. S. Hayashi (Kyoto University) for fruitful collaborations in the study of the color-tuning mechanism of retinal proteins. This study was supported by a Grant-in-Aid for Creative Scientific Research from the Ministry of Education, Culture, Sports, Sciences, and Technology of Japan. A part of the computations was performed in the Research Center for Computational Science, Okazaki, Japan.

REFERENCES

1. Michel-Beyerle ME (ed) (1985) Antennas and Reaction Centers of Photosynthetic Bacteria. Springer-Verlag, Berlin.
2. Deisenhofer J, Norris JR (eds) (1993) The Photosynthetic Reaction Center, Vols I and II. Academic Press, New York.
3. Voet D, Voet JG (1997) Biochemisty, John Wiley & Sons, Inc., New York.
4. Mathies RA, Lin SW, Ames JB, Pollard WT (1991) Annu Rev Biophys Chem 20: 491.
5. Rothschild KJ (1992) J Bioenerg Biomembr 24: 147.
6. Khorana HG (1992) J Biol Chem 267: 1.
7. Hofmann K-P, Helmreich EJM (1996) Biochim Biophys Acta 1286: 285.
8. Schichida Y, Imai H (1998) CMLS, Cell Mol Life Sci 54: 1299.
9. Kendrick RE, Kronenberg GHM (eds) (1994) Photomorphogenesis in Plants. Kluwer Academic Publishers, Dordrecht, The Netherlands.
10. Wood KV, Lam YA, Seliger HH, McElroy WD (1989) Science 244: 700.
11. Shimomura O, Johnson FH, Saiga Y (1962) J Cell Comp Physiol 59: 223.
12. Tsien RY (1998) Annu Rev Biochem 67: 509.
13. Nakatsuji H, Hirao K (1977) Chem Phys Lett 47: 569.
14. Nakatsuji H, Hirao K (1978) J Chem Phys 68: 2053.
15. Nakatsuji H (1978) Chem Phys Lett 59: 362.
16. Nakatsuji H (1979) Chem Phys Lett 67: 329.
17. Nakatsuji H (1979) Chem Phys Lett 67: 334.
18. Nakatsuji H (1991) Chem Phys Lett 177: 331.
19. Nakatsuji H (1992) Acta Chim Hungarica, Models in Chemistry 129: 719.
20. Nakatsuji H (1997) In: J. Leszczynski (ed) Computational Chemistry – Reviews of Current Trends, Vol. 2, World Scientific, Singapore, p 62.
21. Ehara M, Ishida M, Toyota K, Nakatsuji H (2002) In: K.D. Sen (ed) Reviews in Modern Quantum Chemistry, World Scientific, Singapore, p 293.
22. Ehara M, Hasegawa J, Nakatsuji H (2005) In: C.E. Dykstra, G. Frenking, K.S. Kim, G.E. Scuseria (eds) Theory and Applications of Computational Chemistry: The First 40 Years, A Volume of Technical and Historical Perspectives, Elsevier Science.
23. Nakajima T, Nakatsuji H (1997) Chem Phys Lett 280: 79.

24. Nakajima T, Nakatsuji H (1999) Chem Phys 242: 177.
25. Ishida M, Toyoda K, Ehara M, Nakatsuji H (2001) Chem Phys Lett 350: 351.
26. Ishida M, Ehara M, Nakatsuji H (2002) J Chem Phys 116: 1934.
27. Ishida M, Toyoda K, Ehara M, Nakatsuji H (2001) Chem Phys Lett 347: 493.
28. Frisch MJ, Trucks GW, Schlegel HB, Scuseria GE, Robb MA, Cheeseman JR, J. A. Montgomery J, Vreven T, Kudin KN, Burant JC, Millam JM, Iyengar SS, Tomasi J, Barone V, Mennucci B, Cossi M, Scalmani G, Rega N, Petersson GA, Nakatsuji H, Hada M, Ehara M, Toyota K, Fukuda R, Hasegawa J, Ishida M, Nakajima T, Honda Y, Kitao O, Nakai H, Klene M, Li X, Knox JE, Hratchian HP, Cross JB, Adamo C, Jaramillo J, Gomperts R, Stratmann RE, Yazyev O, Cammi R, Pomelli C, Ochterski J, Ayala PY, Morokuma K, Hase WL, Voth G, Salvador P, Dannenberg JJ, Zakrzewski VG, Dapprich S, Daniels AD, Strain MC, Farkas O, Malick DK, Rabuck AD, Raghavachari K, Foresman JB, Ortiz JV, Cui Q, Baboul AG, Clifford S, Cioslowski J, Stefanov BB, Liu G, Liashenko A, Piskorz P, Komaromi I, Martin RL, Fox DJ, Keith T, Al-Laham MA, Peng CY, Nanayakkara A, Challacombe M, Gill PMW, Johnson B, Chen W, Wong MW, Gonzalez C, Pople JA (2003) Gaussian Development Version (Revision A.03). Gaussian, Inc., Pittsburgh PA.
29. Nakatsuji H (1983) Chem Phys 75: 425.
30. Cizek J (1966) J Chem Phys 45: 4256.
31. Cizek J (1969) Adv Chem Phys 14: 35.
32. Ohtsuka Y, Nakatsuji H (2006) J Chem Phys 124: 054110.
33. Nakatsuji H, Hirao K, Mizukami Y (1991) Chem Phys Lett 179: 555.
34. Nakatsuji H (1986) Program Library SAC85 (No. 1396). Computer Center of the Institute for Molecular Science, Okazaki, Japan.
35. Hasegawa J, Fujimoto K, Swerts B, Miyahara T, Nakatsuji H (2007) J Comp Chem 28: 2443.
36. Dunning TH, Hay PJ (1977) In: H.F. Schaefer (ed) Methods of electronic structure theory, III, Prenum Press, New York.
37. Vigny P, Duquesne M (1976) In: J.B. Briks (ed) Excited states of Biological Molecules, Wiley, New York, p 167.
38. Crespo-Hernández CE, Cohen B, Hare PM, Kohler B (2004) Chem Rev 104: 1977.
39. Sancar A (2003) Chem Rev 103: 2203.
40. Kelley SO, Barton JK (1998) Chem Biol 5: 413.
41. Berova N, Nakanishi K, Woody RW (eds) (2000) Circular Dichroism : Principles and Applications, 2nd ed. Wiley-VCH New York.
42. Miles DW, Robins RK, Eyring H (1967) Proc Natl Acad Sci USA 57: 1139.
43. Bureekaew S, Hasegawa J, Nakatsuji H (2006) Chem Phys Lett 425: 367.
44. Hansen AE, Bouman TD (1980) Adv Chem Phys 44: 545.
45. Becke AD (1993) J Chem Phys 98: 5648.
46. Lee C, Yang W, Parr RG (1988) Phys Rev B 37: 785.
47. Hehre WJ, Ditchfield R, Pople JA (1972) J Chem Phys 56: 2257.
48. Hariharan PC, Pople JA (1973) Theor Chim Acta 28: 213.
49. Dunning TH (1971) J Chem Phys 55: 716.
50. Huzinaga S, Andzelm J, Krovkowski M, Radzio-Andzelm E, Sakai Y, Tatewaki H (1984) Gaussian basis set for molecular calculation, Elsevier, New York.
51. Dunning TH (1970) J Chem Phys 53: 2823.
52. Kelly JM, Lagarias JC (1985) Biochemistry 24: 6003.
53. Eilfeld P, Rüdiger WZ (1985) Naturforsch 40c: 109.
54. Fodor SPA, Lagarias JC, Mathies RA (1990) Biochemistry 29: 11141.
55. Andel III F, Lagarias JC, Mathies RA (1996) Biochemistry 35: 15997.

56. Andel III F, Murphy JT, Haas JA, McDowell MT, van der Hoef I, Lugtenburg J, Lagarias JC, Mathies RA (2000) Biochemistry 39: 2667.
57. Farrens DL, Holt RE, Rospendowski BN, Song P-S, Cotton TM (1989) J Am Chem Soc 111: 9162.
58. Tokutomi S, Mizutani Y, Anni H, Kitagawa T (1990) FEBS 269: 341.
59. Kneip C, Hildebrandt P, Schlamann W, Braslavsky SE, Mark F, Schaffner K (1999) Biochemistry 38: 15185.
60. Lippitsch ME, Hermann G, Brunner H, Mueller E, Aussenegg FR (1993) J Photochem Photobiol B 18: 17.
61. Parr RG, Yang W (1989) Density-Functional Theory of Atoms and Molecules, Oxford Univ. Press, Oxford.
62. Zhang C-F, Farrens DL, Björling SC, Song P-S, Kliger DS (1992) J Am Chem Soc 114: 4569.
63. Björling SC, Zhang C-F, Farrens DL, Song P-S, Kliger DS (1992) J Am Chem Soc 114: 4581.
64. Rüdiger W, Thümmler F, Cmiel E, Schneider S (1983) Proc Natl Acad Sci USA. 80: 6244.
65. Kirmaier C, Holten D, Parson WW (1985) Biochim Biophys Acta 810: 49.
66. Nakatsuji H, Hasegawa J, Ohkawa K (1998) Chem Phys Lett 296: 499.
67. Hasegawa J, Ohkawa K, Nakatsuji H (1998) J Phys Chem B 102: 10410.
68. Hasegawa J, Nakatsuji H (1998) J Phys Chem B 102: 10420.
69. Hasegawa J, Nakatsuji H (2005) Chem Lett 34: 1242.0.
70. Deisenhofer J, Epp O, Miki K, Huber R, Michel H (1985) J Mol Biol 180: 385.
71. Katona G, Andersson U, Randau EM, Andersson L-E, Neutze R (2003) J Mol Biol 331: 681.
72. Cornell WD, Cieplak P, Bayly CI, Gould IR, K. M. Merz J, Ferguson DM, Spellmeyer DC, Fox T, Caldwell JW, Kollman PA (1995) J Am Chem Soc 117: 5179.
73. Schmidt S, Arlt T, Hamm P, Huber H, Nägele T, Wachtveitl J, Meyer M, Scheer H, Zinth W (1994) Chem Phys Lett 223: 116.
74. Kandori H, Schichida Y, Yoshisawa T (2001) Biochemistry (Moscow) 66: 1197.
75. Mathies RA, Lugtenburg J (2000) In: D.G. Stavenga, W.J.d. Grip, E.N. Pugh (eds) Handbook of Biological Physics, Elsevier Science B. V., Amsterdam.
76. Kleinschmidt J, Harosi FI (1992) Proc Natl Acad Sci USA 89: 9181.
77. Hayashi S, Ohmine I (2000) J Phys Chem B 104: 10678.
78. Hayashi S, Tajkhorshid E, Pebay-Peyroula E, Royant A, Landau EM, Navarro J, Schulten K (2001) J Phys Chem B 105: 10124.
79. Schreiber M, Buss V, Sugihara M (2003) J Chem Phys 119: 12045.
80. Vreven T, Morokuma K (2003) Theor Chem Acc 109: 125.
81. Ferré N, Olivucci M (2003) J Am Chem Soc 125: 6868.
82. Gascon JA, Batista VS (2004) Biophys J 87: 2931.
83. Hufen J, Sugihara M, Buss V (2004) J Phys Chem B 108: 20419.
84. Wanko M, Hoffmann M, Strodel P, Koslowski A, Thiel W, Neese F, Frauenheim T, Elstner M (2005) J Phys Chem B 109: 3606.
85. Fujimoto K, Hasegawa J, Hayashi S, Kato S, Nakatsuji H (2005) Chem Phys Lett 414: 239.
86. Fujimoto K, Hayashi S, Hasegawa J, Nakatsuji H (2006) J Chem Theory Comput 3: 605.
87. Fujimoto K, Hasegawa J, Hayashi S, Nakatsuji H (2006) Chem Phys Lett 423: 252.
88. Nakayama K, Nakano H, Hirao K (1998) Int J Quantum Chem 66: 157.
89. Wang J, Cieplak P, Kollman PA (2000) J Comput Chem 21: 1049.
90. Lin SW, Imamoto Y, Fukuda Y, Shichida Y, Yoshizawa T, Mathies RA (1994) Biochemistry 33: 2151.
91. Kochendoerfer GG, Wang Z, Oprian DD, Mathies RA (1997) Biochemistry 36: 6577.
92. Morin JG, Hastings JW (1971) J Cell Physiol 77: 313.

93. Morise H, Shimomura O, Johnson FH, Winant J (1974) J Biochem 13: 2656.
94. Ward WW (1979) Photochem Photobiol Rev 4: 1.
95. Inouye S, Tsuji FI (1994) FEBS Lett 341: 277.
96. Zimmer M (2002) Chem Rev 102: 759.
97. Voityuk AA, Michel-Beyerle M-E, Rosch N (1998) Chem Phys Lett 296: 269.
98. Voityuk AA, Michel-Beyerle M-E, Rosch N (1998) Chem Phys 231: 13.
99. Voityuk AA, Kummer AD, Michel-Beyerle M-E, Rosch N (2001) Chem Phys 269: 83.
100. Helms V, Winstead C, Langhoff PW (2000) J Mol Struct (THEOCHEM) 506: 179.
101. Laino T, Nifosi R, Tozzini V (2004) Chem Phys 298: 17.
102. Weber W, Helms V, McCammon JA, Langhoff PW (1999) Proc Natl Acad Sci USA 96: 6177.
103. Das AK, Hasegawa J, Miyahara T, Ehara M, Nakatsuji H (2003) J. Comput. Chem. 24: 1421.
104. Sinicropi A, Andruniow T, Ferre N, Basosi R, Olivucci M (2005) J Am Chem Soc 127: 11534.
105. Martin ME, Negri F, Olivucci M (2004) J Am Chem Soc 126: 5452.
106. Toniolo A, Granucci G, Martinez TJ (2003) J Phys Chem A 107: 3822.
107. Toniolo A, Olsen S, Manohar L, Martinez TJ (2004) Faraday Discuss 127: 149.
108. Lopez X, Marques MAL, Castro R, Rubio A (2005) J Am Chem Soc 127: 12329.
109. Demachy I, Ridard J, Laguitton-Pasquier H, Durnerin E, Vallverdu G, Archirel P, Levy B (2005) J Phys Chem B 109: 24121.
110. Marques MAL, López X, Varsano D, Castro A, Rubio A (2003) Phys Rev Lett 90: 258101.
111. Chattoraj M, King BA, Bublitz GU, Boxer SG (1996) Proc Natl Acad Sci USA 93: 8362.
112. Chalfie M, Tu Y, Euskirchen G, Ward WW, Prasher DC (1994) Science 263: 802.
113. van Thor JJ, Gensch T, Hellingwerr KH, Johnson LN (2002) Nat Struct Biol 9: 37.
114. Volkmer A, Subramaniam V, Birch DJS, Jovin TM (2000) Biophys J 78: 1589.
115. Xu C, Zipfel W, Shear JB, Williams RM, Webb WW (1996) Natl Acad Sci USA 93: 10763.
116. Heim R, Prasher DC, Tsien RY (1994) Proc Natl Acad Sci USA 91: 12501.
117. Cubitt AB, Heim R, Adams SR, Boyd AE, Gross LA, Tsien RY (1995) Trends Biochem Sci 20: 448.
118. Wachter RM, King BA, Heim R, Kallio K, Tsien RY, Boxer SG, Remington SJ (1997) Biochemistry 36: 9759.
119. Bae JH, Rubini M, Jung G, Wiegand G, Seifert MHJ, Azim MK, Kim J, Zumbusch A, Holak TA, Moroder L, Huber R, Budisa N (2002) J Mol Biol 328: 1071.
120. Greer III LF, Szalay AA (2002) Luminescence 17: 43.
121. McCapra F (1977) J Chem Soc Chem Commun 946.
122. Koo J-Y, Schmidt SP, Schuster GB (1978) Proc Natl Acad Sci USA 75: 30.
123. Schuster GB (1979) Acc Chem Res 12: 366.
124. Deluca M (1976) Adv Enzymol 44: 37.
125. White EH, Rapaport E, Seliger HH, Hopkins TA (1971) Bioorg Chem 92.
126. White EH, Rapaport E, Hopkins TA, Seliger HH (1969) J Am Chem Soc 91: 2178.
127. White EH, Steinmetz MG, Miano JD, Wildes PD, Morland R (1980) J Am Chem Soc 102: 3199.
128. Branchini BR, Murtiashaw MH, Magrar RA, Portier NC, Ruggiero MC, Stroh JG (2002) J Am Chem Soc 124: 2112.
129. Branchini BR, Southworth TL, Murtiashaw MH, Magyer RA, Gonzalez SA, Ruggiero MC, Stroh JG (2004) Biochemistry 43: 7255.
130. Miertus S, Scrocco E, Tomasi J (1981) J Chem Phys 55: 117.
131. Nakatani N, Hasegawa J, Nakatsuji H (2007) J Am Chem Soc 129: 8756.
132. Conti E, Franks NP, Brick P (1996) Structure 4: 287.
133. Branchini BR, Magyar RA, Murtiashaw MH, Anderson SM, Zimmer M (1998) Biochemistry 37: 15311.

134. Branchini BR, Magyar RA, Murtiashaw MH, Anderson SM, Helgerson LC, Zimmer M (1999) Biochemistry 38: 13223.
135. Branchini BR, Southworth TL, Murtiashaw MH, Boije H, Fleet SE (2003) Biochemistry 42: 10429.
136. Ugarova NN, Brovko LY (2002) Luminescence 321:
137. Gandelman OA, Brovko LY, Ugarova NN, Chikishev AY, Shkurimov AP (1993) J Photochem Photobiol B: Photobiology 19: 187.
138. Orlova G, Goddard JD, Brovko LY (2003) J Am Chem Soc 125: 6962.
139. Sugihara M, Hufen J, Buss V (2006) Biochemistry 45: 801.
140. Andruniów T, Ferré N, Olivucci M (2004) Proc Natl Acad Sci USA 101: 17908.
141. Stavenga DG, Grip WJ, Pugh EN (2000) In: Molecular Mechanisms in Viral Transduction, Elsevier Science, New York.
142. Birge RR, Zhang CF (1990) J Chem Phys 92: 7178.
143. Balashov SP, Govindjee R, Kono M, Imasheva E, Lukashev E, Ebrey TG, Crouch RK, Menick DR, Feng Y (1993) Biochemistry 32: 10331.
144. Chizhov I, Schmies G, Seidel R, Sydor JR, Lüttenberg B, Engelhard M (1998) Biophys J 75: 999.
145. Ikeura Y, Shimono K, Iwamoto M, Sudo Y, Kamo N (2003) Photochem Photobiol 77: 96.
146. Breton J (1985) Biochim Biophys Acta 810: 235.
147. DeLuca M (1969) Biochemistry 8: 160.